Acta Pharmaceutica Sinica B 2024;14(9):4001−4013

Chinese Pharmaceutical Association
Institute of Materia Medica, Chinese Academy of Medical Sciences

Acta Pharmaceutica Sinica B

www.elsevier.com/locate/apsb
www.sciencedirect.com

ORIGINAL ARTICLE

Molecular glue triggers degradation of PHGDH by enhancing the interaction between DDB1 and PHGDH

Ziqi Huang [a,†], Kun Zhang [a,†], Yurui Jiang [a], Mengmeng Wang [a], Mei Li [a], Yuda Guo [a], Ruolin Gao [a], Ning Li [a], Chenyang Wang [a], Jia Chen [a], Jiefu Wang [b,*], Ning Liu [a,*], Xiang Liu [a,*], Shuangwei Liu [a,*], Mingming Wei [a,*], Cheng Yang [a,*], Guang Yang [a,*]

[a]*The State Key Laboratory of Medicinal Chemical Biology, College of Life Sciences, College of Pharmacy, Nankai University, Tianjin 300071, China*
[b]*Tianjin Medical University Cancer Institute and Hospital, National Clinical Research Center for Cancer, Tianjin's Clinical Research Center for Cancer, Key Laboratory of Cancer Prevention and Therapy, Tianjin 300060, China*

Received 6 February 2024; received in revised form 6 May 2024; accepted 20 May 2024

KEY WORDS

Molecular glue;
Targeted protein degradation;
PHGDH;
Cancer stem cells;
PROTACs

Abstract Cancer stem cells (CSCs) play a pivotal role in tumor initiation, proliferation, metastasis, drug resistance, and recurrence. Consequently, targeting CSCs has emerged as a promising avenue for cancer therapy. Recently, 3-phosphoglycerate dehydrogenase (PHGDH) has been identified as being intricately associated with the regulation of numerous cancer stem cells. Yet, reports detailing the functional regulators of PHGDH that can mitigate the stemness across cancer types are limited. In this study, the novel "molecular glue" LXH-3-71 was identified, and it robustly induced degradation of PHGDH, thereby modulating the stemness of colorectal cancer cells (CRCs) both *in vitro* and *in vivo*. Remarkably, LXH-3-71 was observed to form a dynamic chimera, between PHGDH and the DDB1-CRL E3 ligase. These insights not only elucidate the anti-CSCs mechanism of the lead compound but also suggest that degradation of PHGDH may be a more viable therapeutic strategy than the development of PHGDH inhibitors. Additionally, compound LXH-3-71 was leveraged as a novel ligand for the DDB1-CRL E3 ligase, facilitating the development of new PROTAC molecules targeting EGFR and CDK4 degradation.

*Corresponding authors.
E-mail addresses: jwang05@tmu.edu.cn (Jiefu Wang), liuning@nankai.edu.cn (Ning Liu), liux@nankai.edu.cn (Xiang Liu), 1542366958@qq.com (Shuangwei Liu), mingmingshengwu@163.com (Mingming Wei), Cheng.yang@nankai.edu.cn (Cheng Yang), Guang.yang@nankai.edu.cn (Guang Yang).
[†]These authors made equal contributions to this work.
Peer review under the responsibility of Chinese Pharmaceutical Association and Institute of Materia Medica, Chinese Academy of Medical Sciences.

https://doi.org/10.1016/j.apsb.2024.06.001

1. Introduction

Colorectal cancer (CRC) is the second leading cancer type, accompanied by a pronounced mortality rate[1,2]. While treatments like chemotherapy and radiotherapy can be beneficial for CRC patients' post-surgery, the menace of recurrence remains significant[1]. A distinct subset of cells, termed as colorectal cancer stem cells (CRCSCs), is present within CRC[3,4]. These cells are characterized by their unique ability for self-renewal[3−5]. Several research initiatives[6,7] suggest that CRCSCs play an integral role in tumor initiation, drug resistance[8], facilitating metastasis[9,10], and leading to relapse[11]. Alarmingly, certain therapeutic approaches like chemotherapy and radiotherapy might inadvertently enhance the CRCSCs population. However, a deep understanding of how to modulate the self-renewal, proliferation, differentiation and drug resistance of CRCSCs remains elusive[12].

The enzyme 3-phosphoglycerate dehydrogenase (PHGDH) plays a crucial initial role in the serine biosynthetic pathway, diverging from glycolysis. Using NAD as a cofactor, PHGDH oxidizes the glycolytic compound 3-phosphoglycerate to produce phosphohydroxypyruvate[13,14]. Successive enzymatic reactions in this pathway, namely by PSAT1 through transamination and PSPH during phosphate ester hydrolysis, eventually lead to the formation of serine[15]. To date, a growing body of evidence has demonstrated the prevalent overexpression of PHGDH in various cancer types, underpinning its pivotal role in tumor initiation, invasion and metastasis, drug resistance, and recurrence[16-19]. Consequently, PHGDH has emerged as a promising target, garnering substantial interest from medicinal chemists and biotechnology companies in the development of innovative anti-cancer molecules[20-23].

Previously, the research group identified a novel class of compounds derived from oleanolic acids, exhibiting potent anti-cancer stem cell activities across a broad spectrum of malignant tumors[24]. In the current study, the design and utilization of a pair of "differentiated active molecular probes" enabled the accurate identification of the direct target of the lead compound, LXH-3-71. Particularly, evidence substantiated that this compound could covalently bind to Cys281 of PHGDH, subsequently instigating a ubiquitin-proteasome system (UPS)-mediated degradation of this protein. Further results affirmed that LXH-3-71 acted as a novel "molecular glue", facilitating dynamic proteolysis chimeras composed of PHGDH and DDB1-CRL E3 ligase. Notably, these findings also uncovered that selective degradation of PHGDH might represent a more promising strategy for cancer therapeutics compared to the development of PHGDH inhibitors.

2. Results and discussion

2.1. *LXH-3-71 impairs the proliferation and stemness of colorectal cancer cells in vitro*

Previously, a class of oleanolic acid analogues was identified as compounds with anti-cancer stem cells properties. Upon meticulous validation, the lead compound, LXH-3-71 (Fig. 1A), was selected, because of its potent anti-proliferative and anti-CSC activities against various colorectal cancer cells. Initially, the inhibitory effect of LXH-3-71 against several colorectal cancer cells was assessed through the CCK-8 assay, revealing that the lead compound could significantly inhibit the growth of all selected colorectal cancer cells at low micromolar concentrations (Fig. 1B). To contrast, LXH-3-71 incubationled to demonstrated relatively low cytotoxicity against some human cell lines (Supporting Information Fig. S1). Numerous reports have suggested that metastatic colorectal cancer (mCRC) cells often harbor high stemness, leading to drug resistance, recurrence, and poorer prognosis[25-27]. Subsequent studies determined whether LXH-3-71 could attenuate the stemness of mCRC cells. LXH-3-71 markedly reduced the colony numbers of HCT-116 and SW480 cells grown in soft agar (Fig. 1C−E) and, for selected mCRC cells (HCT-116 and SW480), groups treated with LXH-3-71 not only diminished the sizes of tumorspheres but also reduced the number of tumorspheres in a dose-dependent manner compared to the control group (Fig. 1F−K). Furthermore, LXH-3-71 was found to distinctly inhibit the proliferation of colorectal stem cells ($CD133^+$ and $CD44^+$) sorted by CSC makers in a dose-dependent manner (Fig. 1L and Supporting Information Fig. S2). In summary, these results indicated that LXH-3-71 could notably inhibit the growth of both colorectal cancer cells and colorectal cancer stem cells *in vitro*.

2.2. *LXH-3-71 remarkably inhibits the growth and metathesis of mCRCs in vivo*

Encouraged by promising *in vitro* experimental results, further evaluation of the *in vivo* anti-tumor activity of LXH-3-71 was conducted using mouse xenograft models. First of all, the results pharmacokinetic (PK) studies indicated that IP administration of LXH-3-71 exhibited excellent bioavailability in tested animals. (Please see Supporting Information Fig. S3 and Table S1). Next, in an HCT-116 subcutaneous xenograft model, LXH-3-71 administration effectively inhibited tumor growth in a dose-dependent manner, as illustrated in Fig. 2A−C, and D, and was compared to the reference drug, 5-FU. Negligible changes in body weight of the test animals indicated that both LXH-3-71 and 5-FU were well tolerated (Fig. 2B). Subsequent pathological analysis revealed a significant reduction in Ki67-positive cells in the LXH-3-71 groups, thereby confirming its suppressive impact on tumor proliferation (Fig. 2E). Moreover, the H&E staining of the spleen, liver, kidney and lung tissues showed that LXH-3-71 had none significant systemic toxicity (Supporting Information Fig. S4). Concurrently, an animal model simulating CRC lung metastasis was established to investigate the inhibitory effect of LXH-3-71 on metastatic colonization of CRCs. Mice treated with LXH-3-71 exhibited minimal fluorescence signals compared with the vehicle control and 5-FU treatment groups (Fig. 2F and G), indicating a significant reduction in lung metastatic burden as a result of LXH-3-71 administration. This observation was further substantiated by H&E staining, which demonstrated a notable reduction in lung metastasis following LXH-3-71 treatment (Fig. 2H).

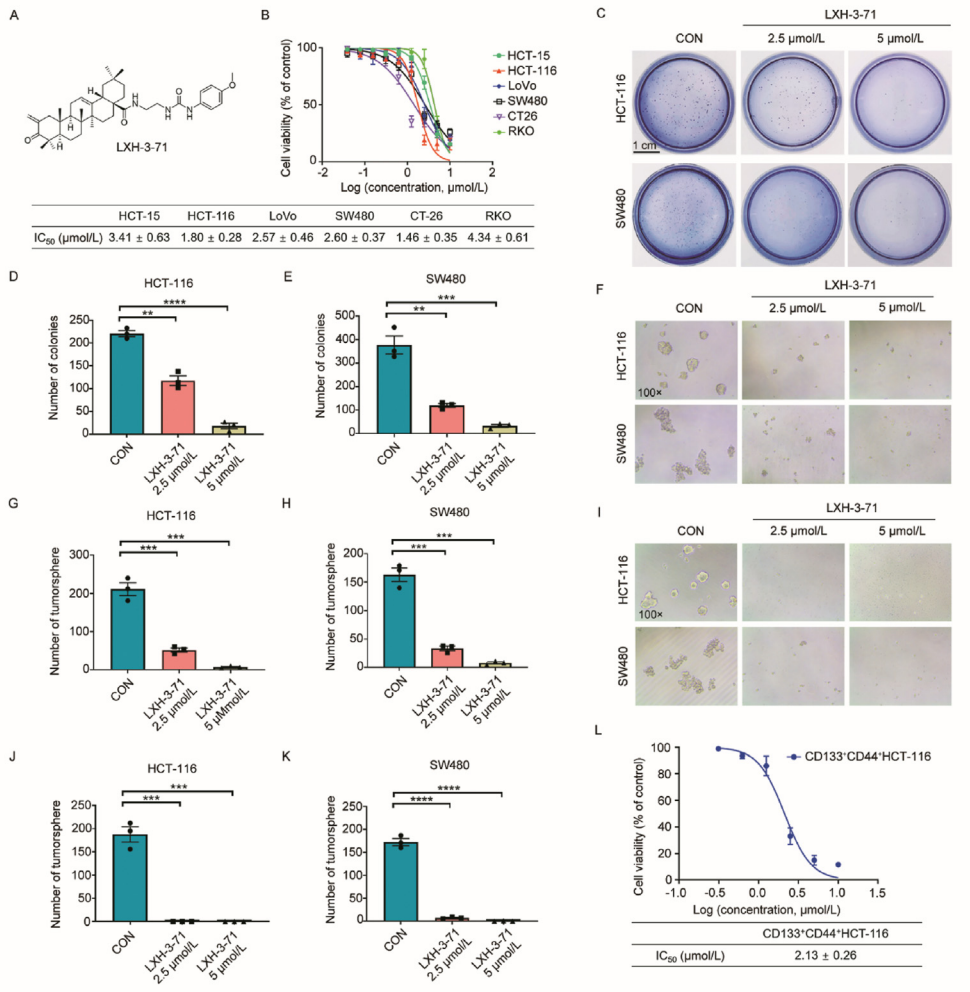

Figure 1 The antiproliferative effects of LXH-3-71 on colorectal cancer cells and associated stem cells under *in vitro* conditions. (A) Chemical structure of lead compound LXH-3-71. (B) IC_{50} curve of lead compound LXH-3-71 against colorectal cancer cell lines. IC_{50} values were calculated using GraphPad Prism software, and were expressed as the mean ± SD of three independent experiments. (C) Inhibition of LXH-3-71 on the colony formation of colorectal cancer cells on soft agar. (D and E) Quantification of soft agar assay from (C). (F) Representative fields of tumorspheres treated by indicated concentrations of LXH-3-71 or DMSO for 72 h. (G and H) Quantitative analysis of the number of tumorspheres from (F). (I) Representative images of tumorspheres formed form HCT-116 and SW480 cells pre-treated with LXH-3−71 (2.5 and 5 μmol/L) or DMSO for 3 days. (J, K) Quantitative analysis of the number of tumorspheres from (I). (L) Cell viability inhibition of LXH-3-71 on $CD133^+$ $CD44^+$ HCT-116 cells, and IC_{50} value (mean ± SD) was determined in triplicate. Statistical significance was determined by unpaired *t*-test. Error bars denoted SEM, $n = 3$, $^{**}P < 0.01$, $^{***}P < 0.001$, $^{****}P < 0.0001$.

2.3. *Design, synthesize and screen for differentiated chemical probes derived from LXH-3-71*

The combined outcomes from previous investigations strongly imply that LXH-3-71 possesses significant efficacy against CRCSCs, both within laboratory settings and *in vivo* models. To further delve into the precise mechanism whereby LXH-3-71 counters the inherent stemness traits of mCRC cells, we designed and synthesized specific chemical probes, as depicted in Fig. 3A, to facilitate advanced affinity pull-down studies. It's increasingly recognized in scientific literature that moieties with α,β-unsaturated enone configurations can act as Michael acceptors. These configurations readily engage in forming a covalent C−S linkage with distinct cysteine regions within the target protein[28,29]. Consequently, chemical probes, both with and without enone moieties, were developed through straightforward synthesis steps (Supporting Information Scheme S1). Additionally, biological evaluation results revealed that probe **10**, which bears an enone moiety, maintained potent anti-CRCSCs activity at nearly 5 μmol/L, whereas its analogue, **13**, exhibited no activity (Fig. 3B and C).

2.4. *LXH-3-71 could covalently bind to Cys281 of PHGDH*

Employing these "differentiated active chemical probes", subsequent "pull-down" experiments were conducted to identify the proteins which the active probe selectively bound to sustain its anti-CRCSC activity. To achieve that, HCT-116 cell lysates were incubated with the pair of probe molecules that were previously linked with streptavidin-containing beads. The bound proteins were precipitated, washed with buffers, resolved *via* SDS-PAGE, and subsequently stained. According to Fig. 3D, a distinct band,

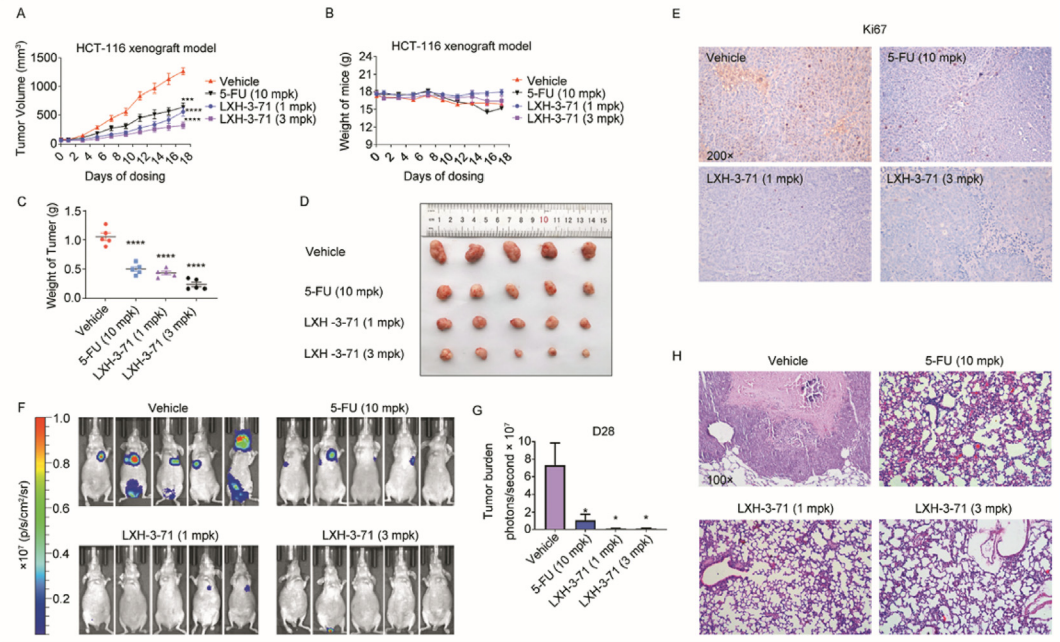

Figure 2 Effect of LXH-3-71 (1 and 3 mpk, i.p, QD) on CRC growth and metastatic potential *in vivo*. (A) Alterations in tumor volume throughout the administration in xenograft models. (B) Fluctuations in mice body weight during the treatment period in xenograft models. (C) Quantification of tumor weight across four groups upon sacrifice of mice. (D) Images of tumors excised from xenograft models on Day 17. (E) Tumor sections immunostained with anti-Ki67 antibody and imaged at 200× magnification. (F) Bioluminescence imaging of a lung metastasis animal model. (G) Quantification of bioluminescence signals for (F). (H) Hematoxylin and eosin (H&E) staining of lung sections. Statistical significance was determined by unpaired *t*-test. Error bars denoted SEM, $n = 5$, $^{*}P < 0.05$, $^{***}P < 0.001$, $^{****}P < 0.0001$.

observed near 55 kDa, was specifically precipitated by positive probe **10** and was identified as PHGDH by LC−MS/MS (Fig. 3E). Subsequent immunoblotting results further indicated that PHGDH was enriched in the precipitates of the positive probe **10** group and was scarcely detected in the negative probe **13** group (Fig. 3F). The provided data suggest a covalent reaction between LXH-3-71 and PHGDH. In our pursuit to pinpoint the exact Cys residue that binds, we subjected the full-length recombinant human PHGDH protein to purification and subsequent incubation with LXH-3-71. Post incubation, trypsin digestion was performed on the samples, followed by an LC−MS/MS (Fushion) analysis. Referring to Fig. 3G, both computations and database searches highlighted a peptide exhibiting a mass of 2648.4499 Da. This weight was precisely 657.4326 Da greater than the mass of the peptide encompassing Cys281, identified as ALVDHENVISCPHLGASTK (with a calculated mass of 1991.0173 Da). Intriguingly, this mass variance (657.4326 Da) seamlessly aligned with the molecular weight of LXH-3-71. Tandem mass spectrometry analyses of the peptide pointed to this unique mass alteration spanning from the y1 to y18 fragment ions, suggesting a covalent interaction of LXH-3-71 with the thiol fraction of the Cys281 residue. However, capturing crystal data remained elusive, possibly due to the protein's pronounced flexibility. Notably, it was further confirmed that Cys281 of PHGDH was essential for maintaining the anti-CSCs activity of LXH-3-71 both *in vitro* and *in vivo* (Supporting Information Fig. S5). Additionally, analysis of the TCGA database revealed a positive correlation between PHGDH and the expression of tumor stem cell-related genes at the mRNA level in both colon and rectal cancers (Fig. 3I). Drawing conclusions from the results, PHGDH emerged as the immediate target of the anti-CSCs lead compound, demonstrating its ability to form a covalent bond at the Cys281 region of the protein.

2.5. *LXH-3-71 triggers significant and selective degradation of PHGDH both in vitro and in vivo*

Initial docking results unexpectedly revealed that the binding site for small molecules on PHGDH constitutes a shallow pocket situated on its surface, ostensibly unrelated to the previously reported catalytic domain of PHGDH[30]. The enzyme activity was initially probed to ascertain whether LXH-3-71 could inhibit PHGDH activity. NCT503, previously reported as a potent PHGDH inhibitor, served as a positive control[31]. Findings indicated that NCT503 presented an IC_{50} value of 7.17 ± 1.80 μmol/L[32], while LXH-3-71 exhibited no inhibitory effect against PHGDH ($IC_{50} > 50$ μmol/L, Fig. 4A and B). Interestingly, NCT503 demonstrated a negligible impact on dispersing the spheroids of CRC cells (see Supporting Information Fig. S6), which suggested that PHGDH might modulate the stemness of CRC cells *via* an enzyme-independent mechanism. Subsequent cellular analyses revealed that LXH-3-71 treatment significantly downregulated PHGDH protein levels in CRC cells in both dose- and time-dependent manners (Fig. 4C and D). Furthermore, quantitative RT-PCR results suggested that LXH-3-71 likely does not impede the transcriptional process (Fig. 4E). Additionally, cycloheximide (CHX) treatment experiments revealed that LXH-3-71 administration could distinctly diminish PHGDH stability (Fig. 4F). Notably, this protein degradation could be counteracted by subsequent administration of MG-132, a potent proteasome inhibitor (Fig. 4G). LXH-3-71 treatment was also found to induce poly-ubiquitination of PHGDH, making it susceptible to

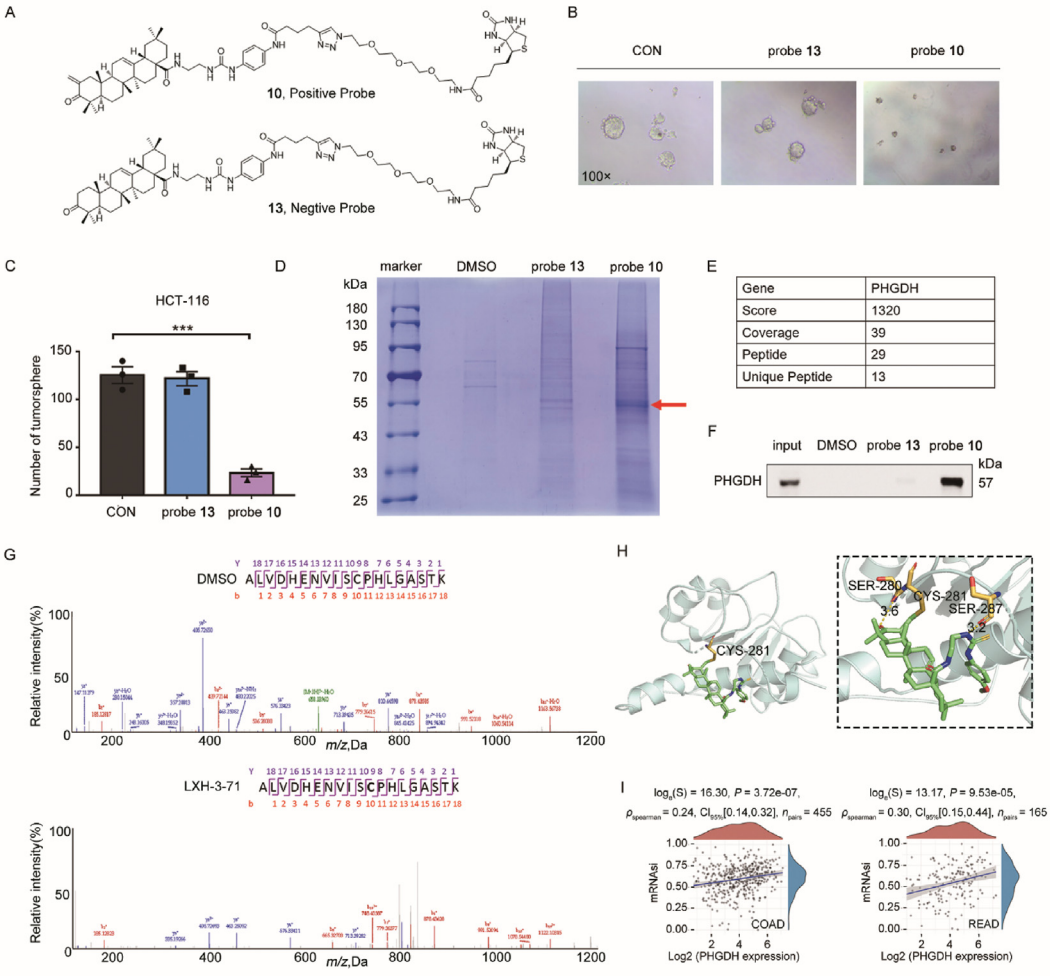

Figure 3 Identification of targeted protein of LXH-3-71 based on chemical probes. (A) Chemical structure of probes originating from LXH-3-71. (B) Representative fields of tumorspheres treated by DMSO, positive probe **10**, and negative probe **13**. (C) Quantitative analysis of the number of tumorspheres form (B). Statistical significance was determined by unpaired *t*-test. Error bars denoted SEM, $n = 3$, $^{***}P < 0.001$. (D) Streptavidin-agarose beads with chemical probes (probe **10**, and probe **13**) were incubated with HCT-116 cell lysates to pull down probes-bound proteins. Proteins were separated by 10% SDS-PAGE and stained with Comassie brilliant blue. (E) Information of targeted protein PHGDH from LC−MS/MS analysis. (F) Binding verification between LXH-3-71 and PHGDH through a combination of pull-down and western blotting approaches in HCT-116 cells. (G) Fusion MS/MS analysis of the recombinant human PHGDH with DMSO and LXH-3-71 incubation, respectively. (H) A hypothetical binding model for the interaction between LXH-3-71 and PHGDH. (I) Spearman analysis evaluated the correlations between PHGDH gene expression and stemness indices, utilizing corresponding clinical information for colon cancer (left) and rectal cancer (right) derived from the TCGA dataset.

proteasomal digestion (Fig. 4H). *In vivo* analyses of CRC tumor tissue samples using western blotting (Fig. 4I) and immunohistochemical staining (IHC) (Fig. 4J) exhibited a conspicuous downregulation of PHGDH levels across all samples following LXH-3-71 treatment. Moreover, selectivity for degradation was evaluated *via* quantitative proteomics analysis, identifying PHGDH as the most significantly downregulated protein (Fig. 4K). In summary, the accumulated data confirm that LXH-3-71 can notably induce the efficient and selective degradation of PHGDH, in both *in vitro* and *in vivo* contexts.

2.6. *PHGDH modulates the stemness of CRCs*

To elucidate the role of PHGDH in regulating the stemness of colorectal cancer cells, lentivirus-mediated shRNA knockdown and overexpression of *PHGDH* were performed in HCT-116 and HCT-15 cells respectively, and the PHGDH expression were validated by Western blot assay (Fig. 5A). Firstly, The proliferative effects of CRC cells were positively regulated by PHGDH alternation (Supporting Information Fig. S7). Tumorsphere formation experiments revealed that, in contrast to the control group, *PHGDH* knockdown significantly impeded cells' capacity to form pellets and diminished the dimensions of the tumorspheres. Conversely, *PHGDH* overexpression enhanced tumorsphere formation and CSCs' self-renewal (Fig. 5B and C). Secondly, *PHGDH* knockdown substantially reduced the frequency of tumorsphere initiation, as evidenced by limited dilution assays (LDA) *in vitro*, while ectopic PHGDH expression notably ameliorated sphere-initiation efficacy (Fig. 5D). Additionally, colony formation assays in soft agar affirmed the attenuation of cell growth upon *PHGDH* depletion, while its

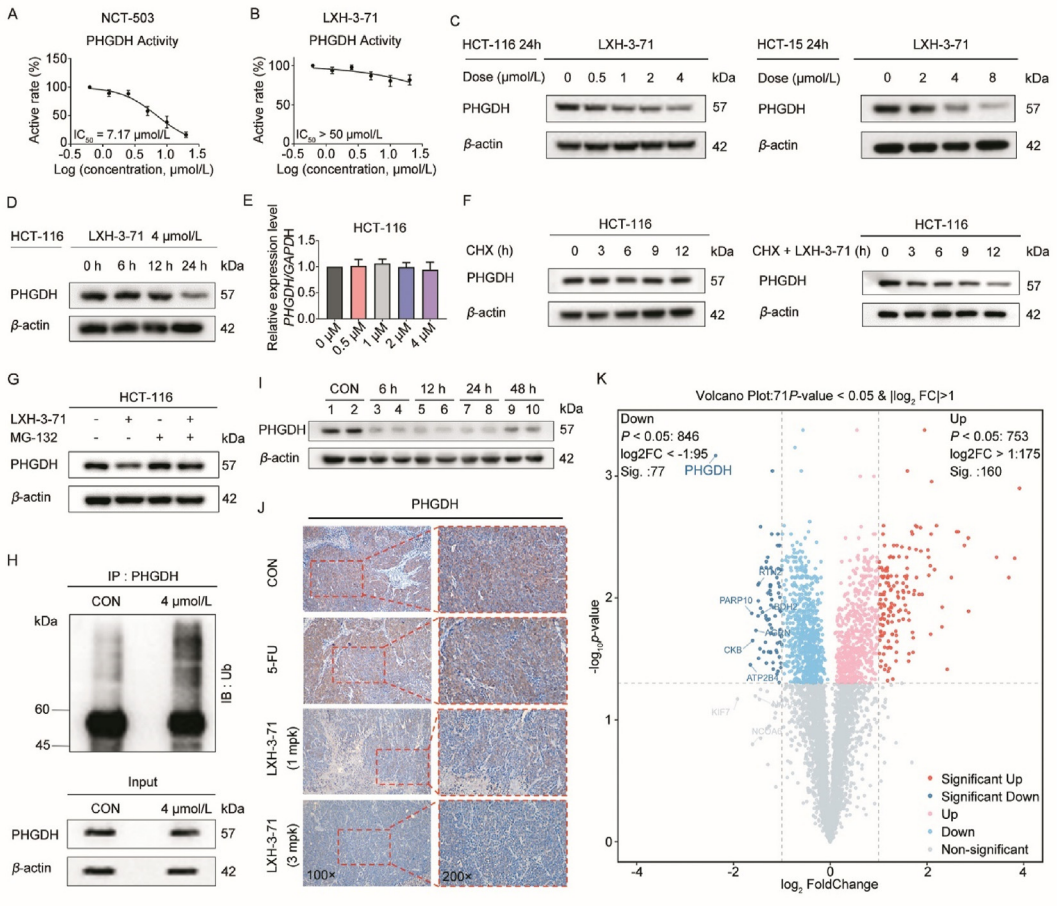

Figure 4 Ubiquitin-dependent PHGDH degradation induced by LXH-3-71. (A and B) Inhibition of PHGDH enzyme activity by NCT-503 and LXH-3-71 conducted with the instruction from PHGDH activity assay kit. IC_{50} values were calculated with GraphPad Prism software. Data were represented as mean ± SD, $n = 3$. (C) Evaluation of PHGDH expression in HCT-116 and HCT-15 cells incubated with the indicated concentrations of LXH-3-71 for 24 h *via* Western blot. (D) Changes analysis of PHGDH protein level in HCT-116 cells treated with LXH-3-71 (4 μmol/L) for indicated time points by Western blot. (E) Detection of PHGDH mRNA levels in HCT-116 cells treated with different concentrations of LXH-3-71 (24 h) by qRT-PCR. Error bars denoted SEM, $n = 3$. (F) Identification of PHGDH protein level in CHX-treated cells with or without LXH-3-71 treatment (4 μmol/L) for indicated time points by Western blot. (G) Western blot analysis of PHGDH protein level in DMSO and LXH-3-71 (4 μmol/L) pre-treated cells (for 18 h) following treatments with MG-132 (10 μmol/L) for 6 h. (H) Western blot analysis of ubiquitin accumulation on PHGDH protein in DMSO and LXH-3-71 (4 μmol/L) pre-treated cells (for 18 h) following treatments with MG-132 (10 μmol/L) for 6 h. (I) Western blot scrutiny of PHGDH levels in tumor tissues from the groups after administration of LXH-3-71 (3 mpk) for indicated time points, compared to vehicle group. (J) Tumor sections from mice treated with vehicle, 5-FU, and LXH-3-71 were subjected to staining using anti-PHGDH antibodies, followed by photographic documentation. (K) A volcano plot depicts the differentially regulated proteins in cells treated with DMSO and LXH-3-71, with the *x*-axis showcasing the $\log_2$-transformed ratio in LXH-3-71 treated cells relative to control cells and the *y*-axis revealing the $-\log_{10}$-transformed *P*-value.

overexpression markedly fostered malignant cloning formation (Fig. 5E and F). Moreover, given that certain colorectal cancer stem cell biomarkers (LGR5, CD44, CD133, and CD166) are pivotal for assessing the stemness of CRCs[33], the influence of PHGDH on the regulation of these genes was examined. Both knockdown and overexpression of *PHGDH* in the HCT-116 cell line resulted in the respective reduction or increment of *LGR5*, *CD44*, *CD133*, and *CD166* mRNA levels, as determined by qRT-PCR (Fig. 5G). Changes in the protein levels of LGR5 and CD44 were also corroborated by Western blotting (Fig. 5H). *PHGDH* knockdown also induced up-regulation of ROS level and down-regulation of GSH/GSSG ratio (Supporting Information Fig. S8). Furthermore, *PHGDH* deletion significantly inhibited tumor growth and diminished the tumor initiation frequency *in vivo*, as demonstrated by *in vivo* LDA experiments (Fig. 5I–L). Then, the xenograft tumor tissue samples were analyzed using Western blotting (Fig. 5M) and IHC staining (Supporting Information Fig. S9). The expression levels of CD133, CD44, LGR5 and CD166 were downregulated in sh-PHGDH group compared with NC group (Fig. 5M). In summary, the results collectively substantiate that PHGDH expression is pivotal for maintaining the stemness of CRCs.

2.7. *LXH-3-71 was identified as a "molecular glue" to furnish dynamic complex composed of PHGDH with DDB1-CUL4 ubiquitin ligase*

To delve deeper into the molecular mechanism of degradation instigated by LXH-3-71, immunoprecipitation was performed a

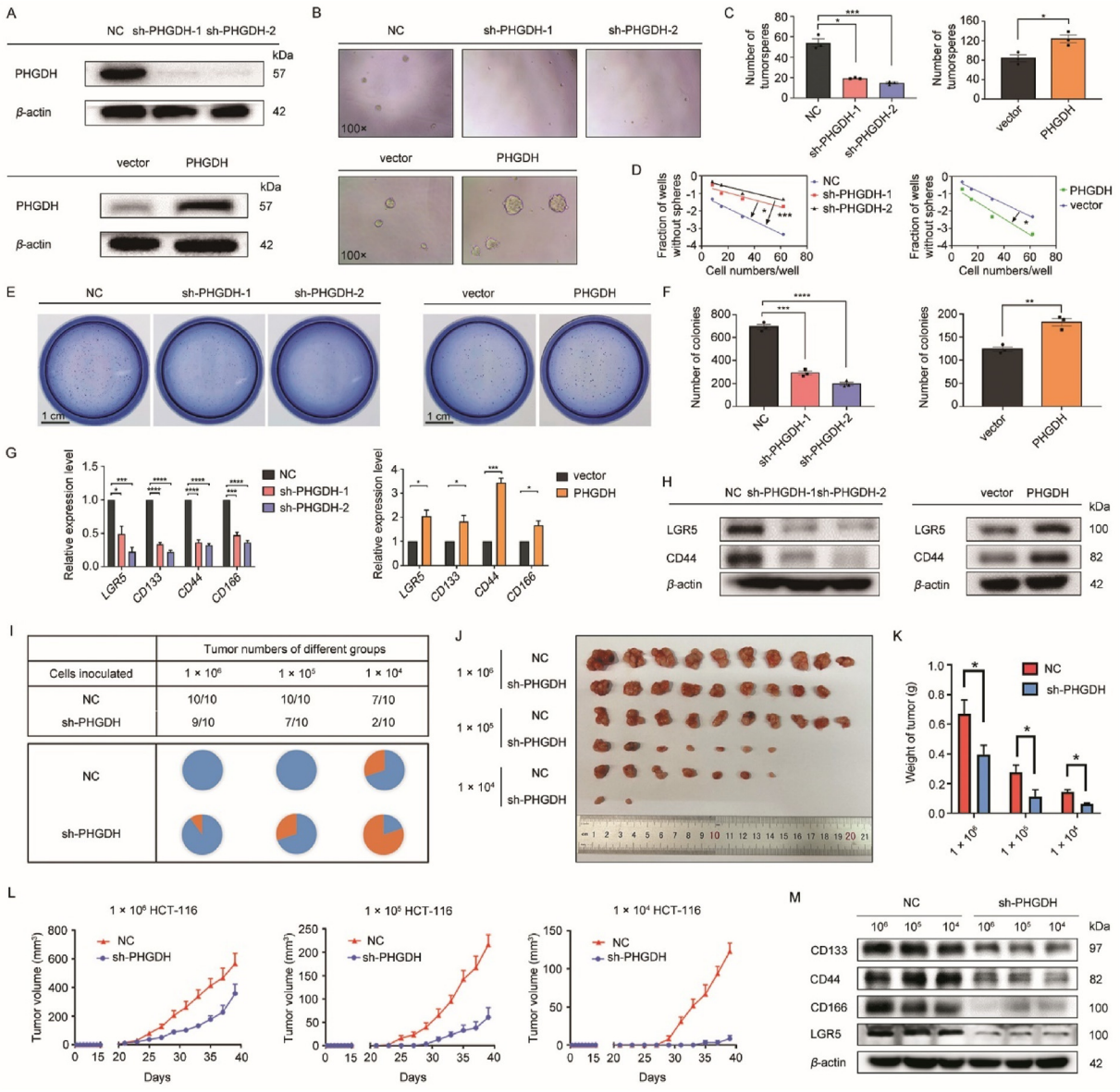

Figure 5 The regulatory role of *PHGDH* in maintaining the stemness of CRC cells. (A) Western blot analysis of PHGDH protein level in HCT-116 cells with stable expression of scrambled or *PHGDH* shRNA, and in parallel or *PHGDH* overexpression HCT-15 cells. (B) Representative micrographs of tumorspheres from HCT-116 cells bearing scrambled or *PHGDH* shRNA (up) or *PHGDH*-overexpression HCT-15 cells (down). (C) Quantification of the numbers of tumorspheres in (B). (D) Limiting dilution analysis (LDA) to assess the sphere-initiation capacity of stable *PHGDH* knockdown or overexpression cells. Cells were planted into 96-well plates at densities of 8, 15, 31, or 62 cells per well and cultured for 10 days, followed by counting of wells containing tumorspheres and analysis utilizing ELDA software. (E) Representative images of colony formation in soft agar. (F) Quantification of colony numbers in (E). (G) Quantitative RT-PCR analysis of CRC stem cell markers *(LGR5*, *CD133*, *CD44*, and *CD166*). (H) Detection of PHGDH protein levels of CD44 and LGR5 by Western blot. (I) Limiting dilution tumorigenesis assays conducted by subcutaneously injecting scrambled or *PHGDH* shRNA cells (1×10^4, 1×10^5, and 1×10^6) into BALB/c nude mice. After 39 days, animals were sacrificed. The ratio of formed tumors to the total number in each group is presented in a table and illustrated in a pie chart. (J) Images of tumors excised from mice injected with scrambled or *PHGDH* shRNA cells. (K) Tumor tissue weight. (L) Tumor volume growth curve for each group. (M) Western blot analysis of CD133, CD44, LGR5 and CD166 level in sh-PHGDH group and NC group. Statistical significance was determined by unpaired *t*-test. Error bars denoted SEM, $^*P < 0.05$, $^{**}P < 0.01$, $^{***}P < 0.001$, $^{****}P < 0.0001$.

PHGDH specific antibody, with or without LXH-3-71 treatment. Upon resolution in SDS-PAGE, a conspicuous band emerged in the LXH-3-71 treatment group, later identified as DDB1 by LC–MS/MS (Fig. 6B and C). DDB1 has been reported as a crucial component of the DDB1-CUL4 ubiquitin ligase complex, wherein, through interaction with adaptor proteins, it facilitates substrate recruitment to the complex for ubiquitination and eventual proteasomal degradation[34-36]. It was posited that LXH-3-71 may serve as a "molecular glue", adhering PHGDH and the DDB1-CUL4 ubiquitin ligase, and conveying poly-ubiquitination to PHGDH. To substantiate this supposition, PHGDH/DDB1 complexes were precipitated and subjected to immunoblotting

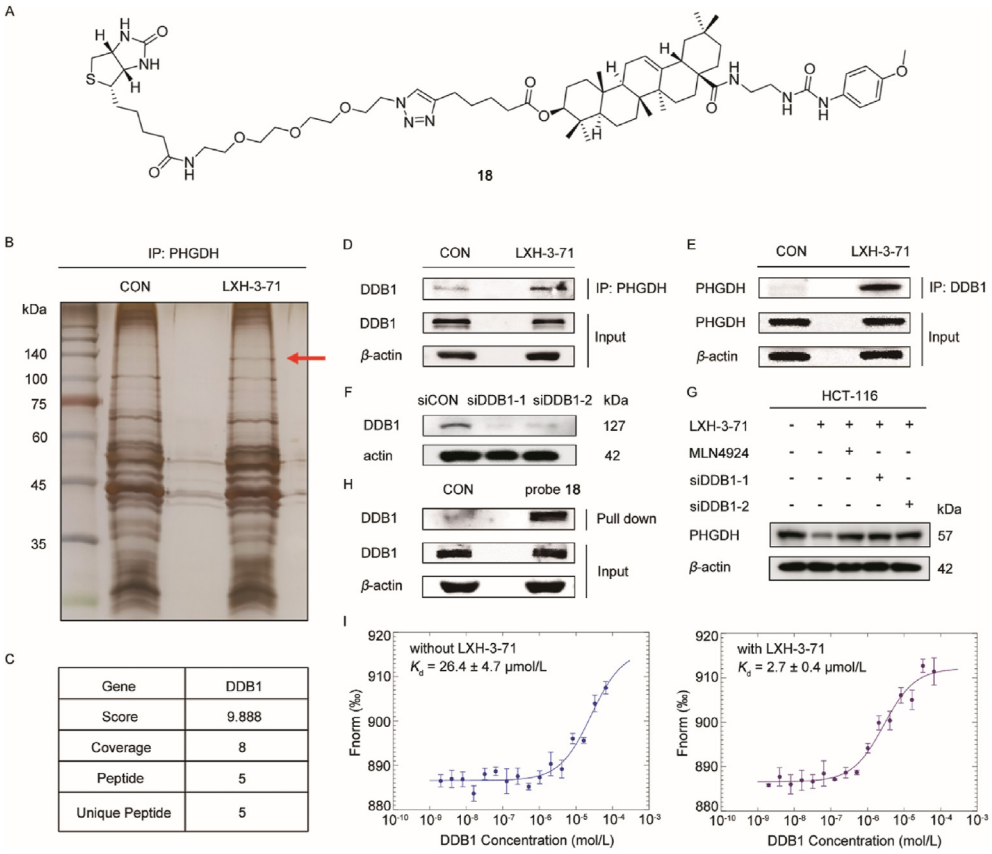

Figure 6 LXH-3-71 functions as a molecular glue facilitating PHGDH-DDB1 Interaction. (A) Chemical structure of compound **18**. (B) Silver staining of immunoprecipitated proteins separated by SDS-PAGE. (C) Data pertaining to the DDB1-CUL4 ubiquitin ligase, derived from LC−MS/MS analysis. (D, E) Co-IP assays were executed utilizing anti-PHGDH and anti-DDB1 antibodies, respectively, followed by Western blot analysis. (F) Western blot analysis of DDB1 protein level in HCT-116 cells transfected with siCON or si*DDB1* oligos. (G) Western blot analysis of PHGDH protein level in MLN4924 (1 μmol/L) or *DDB1* knockdown pre-treated HCT-116 cells followed by treatment with LXH-3-71 for 24 h. (H) A protein affinity pull-down assay, utilizing probe **18**, was conducted with HCT-116 cell lysate and subsequently analyzed through a Western blotting assay. (I) Interaction studies between DDB1 and PHGDH (left) or PHGDH preincubated with LXH-3-71 (right) using microscale thermophoresis method. Data are represented as mean ± SD, $n = 3$.

with anti-PHGDH or anti-DDB1 antibodies, respectively. The findings, illustrated in Fig. 6D and E, indicated that LXH-3-71 treatment markedly amplifies the interaction between PHGDH and DDB1. Subsequently, it was observed that the knockdown of *DDB1* or introduction of MLN4924, a documented specific inhibitor of the DDB1-CUL4 complex, could notably disrupt the LXH-3-71-induced degradation of PHGDH (Fig. 6F and G). Additionally, an alternative biotin-containing probe **18** was designed and synthesized, connecting the biotin from the PHGDH binding site of LXH-3-71 (Fig. 6A). DDB1 was significantly enriched in pull-down experiments with **18** (Fig. 6H). To further verified the formation of dynamic E3 ligase complex *in vitro*, microscale thermophoresis method was used to measure the binding affinity of DDB1 and PHDGH in or out the presence of LXH-3-71. The results were delineated in Fig. 6I, the direct binding potency of DDB1 with PHGDH was weak, and the value of K_d was 26.4 μmol/L. To our delight, the covalent complex of PHGDH and LXH-3-71 (pre-incubated PHGDH with LXH-3-71) was exhibited enhanced binding capability to DDB1 (K_d = 2.7 μmol/L). Notably, the complex of PHGDH^{C281S} and DDB1 could not be facilized by additional of LXH-3-71 (Supporting Information Fig. S10). Additionally, it was also determined that *DDB1* knockdown attenuated anti-proliferation and anti-CSC activities of LXH-3-71 by markedly alleviating degradation of PHGDH (Supporting Information Fig. S11). In summary, these above-findings bolstered the hypothesis that LXH-3-71 substantially induces the formation of a dynamic complex between PHGDH and DDB1-CUL4 ubiquitin ligase, consequently facilitating the efficient cellular proteasomal degradation of PHGDH (Fig. 7).

2.8. LXH-3-71 was utilized for development of new PROTAC molecules to degrade EGFR and CDK4

Based on the elucidation of the crucial mechanism of the "molecular glue" LXH-3-71 for the degradation of PHGDH in CRC cells, the endeavor aimed to chemically convert small molecular drugs into novel PROTAC molecules for targeted protein degradation (TPD), utilizing LXH-3-71 analogues as a novel ligand of E3 ligase. Initially, Gefitinib was selected as the ligand for the target protein in a preliminary attempt to develop a new EGFR degrader. As illustrated in Supporting Information Scheme S2, chemical linkers of varying types and lengths were employed to conjugate the core of Gefitinib with LXH-3-71, resulting in the

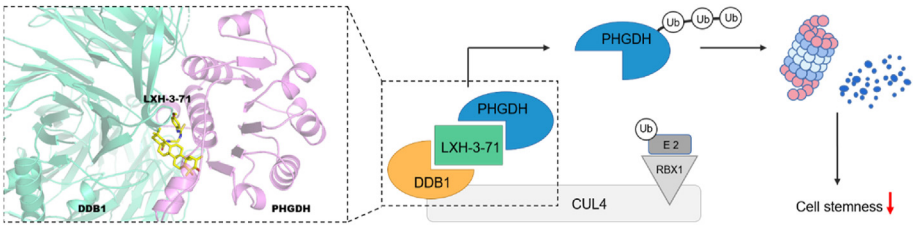

Figure 7 Mechanism of LXH-3-71 as a molecular glue. LXH-3-71 induces the interaction between PHGDH and DDB1-CUL4 ubiquitin ligase, triggering degradation of PHGDH *via* the ubiquitination proteasome pathway and subsequently leading to inhibited cancer cell stemness.

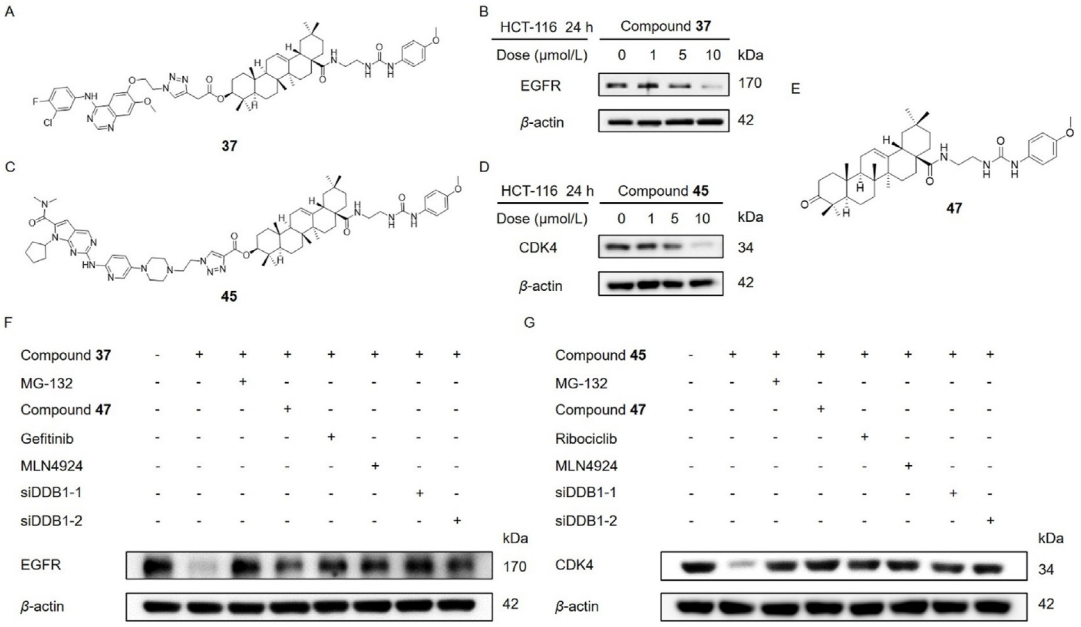

Figure 8 Targeted protein degradation induced by PROTAC derived from LXH-3-71. (A, C) Chemical structures of compounds **37** and **45**, respectively. (B, D) Cells were incubated with either compound **37** or compound **45** at specified concentrations for 24 h, followed by an assessment of targeted protein levels *via* Western blot analysis. (E) Chemical structure of compound **47**. (F) Western blot analysis of EGFR protein level in MG-132 (10 μmol/L), compound **47** (10 μmol/L), Gefitinib (10 μmol/L), MLN4924 (1 μmol/L) or *DDB1* knockdown pre-treated HCT-116 cells followed by treatment with compound **37** for 24 h. (G) Western blot analysis of CDK4 protein level in MG-132 (10 μmol/L), compound **47** (10 μmol/L), Ribociclib (10 μmol/L), MLN4924 (1 μmol/L) or *DDB1* knockdown pre-treated HCT-116 cells followed by treatment with compound **45** for 24 h.

preparation of eight potential TPD molecules. The TPD efficacies of these molecules were biologically evaluated through *in vitro* western blotting within a 24-h frame (Supporting Information Fig. S12). Compound **37** was identified as the most efficient molecule for EGFR degradation, exhibiting efficacy in a dose-dependent manner (Fig. 8A and B). Subsequent to this success in optimizing the chemical linker, a potent CDK4 TPD molecule, **45**, was synthesized and identified, employing the structure of Ribociclib (Supporting Information Scheme S3, Supporting Information Fig. S13, Fig. 8C and D). To verify whether the down-regulation of EGFR and CDK4 were PROTAC-mediated degradation, the HCT-116 cells were firstly pre-incubated with MG-132, compound **47**, Gefitinib and Ribociclib, respectively (Supporting Information Scheme S4, Fig. 8F and G). As revealed from the comparison with DMSO group, the degradations of EGFR and CDK4 triggered by both compounds were obviously attenuated. Without the active proteasome, inhibited by MG-132, the degradation of EGFR and CDK4 were completely inhibited. Since compound **47** was the potential ligand of PHGDH and DDB1, and Gefitinib and Ribociclib were ligands of EGFR and CDK4, respectively, the pre-treatment with high concentrations of these compounds will occupy the pockets of proteins and result in disturbing the formation of ternary complex between DDB1, target proteins and PROTACs, which will significantly inhibit the UPS-mediated degradation of the target proteins. Pre-treated with MLN4924 (CRL inhibitor) or *DDB1* knockdown could also terminate the degradation process of both EGFR and CDK4. Collectively, these findings may offer novel and alternative strategies for the design and discovery of new TPD molecules, which could induce CRL4-mediated protein degradation.

3. Conclusions

In conclusion, the current study unveiled a novel "molecular glue", LXH-3-71, which instigates potent and selective degradation of PHGDH, subsequently modulating the stemness of CRCs both *in vitro* and *in vivo*. It has been observed that LXH-3-71 can facilitate the formation of dynamic complexes, amalgamating PHGDH with DDB1-CUL4 ubiquitin ligase, which consequently induces rapid poly-ubiquitination and proteasomal degradation of

PHGDH. The elimination of PHGDH appears to attenuate the stemness of CRCs in an enzyme-independent manner. These findings not only elucidate the anti-CSCs mechanism of the lead compound but also demonstrate that selective degradation of PHGDH could emerge as a more promising strategy for cancer therapeutics compared to PHGDH enzyme inhibitors. Moreover, this work furnishes a novel ligand of DDB1-CRL E3 ligase, paving the way for designing new PROTAC molecules.

4. Experimental

4.1. Cell culture

The cell lines used in this study were purchased from Procell Life Science&Technology Co., Ltd. Colorectal cancer cell lines (HCT-116, SW480, HCT-15, LoVo, RKO and CT26) and normal cell lines (MCF 10A, BEAS-2B, LO2 and 293T) were incubated at 37 °C in a humidified atmosphere containing 5% CO_2. HCT-116 cells were cultured in McCoy's 5A medium; HCT-15, LoVo and CT26 cells in RPMI1640; SW480, BEAS-2B, LO2 and 293T in Dulbecco's modified Eagle's medium (DMEM) and RKO in MEM. All media were supplemented with 10% fetal bovine serum (FBS, Procell) and 1% penicillin-streptomycin (YEASEN). MCF 10A cells were cultured in DMEM/F12 with 5% HS, 20 ng/mL EGF, 0.5 μg/mL hydrocortisone, 10 μg/mL insulin, 1% NEAA and 1% penicillin-streptomycin.

4.2. Virus production and cell infection

HCT-116 and HCT-15 cells were infected with lentivirus to construct a stable knockdown or overexpression cell line, respectively. Briefly, shRNA fragments were cloned into pLKO.1-puro plasmid using AgeI/EcoRI sites. Full length sequence of human *PHGDH* was synthesized and cloned into pCDH-CMV-MCS-EF1-copGFP vector, which was contracted by HANBIO. For lentivirus production, HEK293FT cells were transfected with recombinant plasmid and the packaging vectors PSPAX2 and pMD2G using polyethylenimine (YEASEN). Medium containing the virus was collected at 24 and 48 h after transfection. HCT-116 or HCT-15 cells were infected with the collected virus supernatant in the presence of 8 μg/mL polybrene (YEASEN). The shRNA sequences were listed as follows:

sh-PHGDH-1: 5′-CCCTGTAGTACAGCAATAA-3′;
sh-PHGDH-2: 5′-CGCAGAACTCACTTGTGGAAT-3′;
sh-DDB1-1: 5′-CGACCGTAAGAAGGTGACTTT-3′;
sh-DDB1-2: 5′-CCTTGATTGGTGTTGCCAGTT-3′.

4.3. Fluorescence activated cell sorting

Flow cytometry was performed to sort $CD133^+$ $CD44^+$ subpopulation form HCT-116 cells. The cells were harvested, washed twice with PBS, and suspended in 500 μL PBS. Cells were then treated with 25 μL FcR Blocking Reagent for 15 min, and incubated with antibodies (human anti-CD44-FITC and human anti-CD133-APC, BD Pharmingen, USA) for 30 min. Subsequently, cells were washed twice with PBS and centrifuged. The cell pellet was resuspended in 100 μL McCoy's 5A medium. $CD133^+CD44^+$ cells were sorted by a cell sorter (BD FACSAria III).

4.4. Cell cytotoxicity assay

CCK-8 assays were used to assess the sensitivity of different cancer cell lines to the drug. Cells were seeded at a density of 5×10^3−8×10^3 cells/well into 96 well-plates. Then, LXH-3-71 was added at different concentrations after 24 h. After drug treatment for 72 h, 10 μL of CCK-8 (Vazyme, A311-01) solution was added to each well and incubated for another 2 h. The absorbance at 450 nm was measured with a microplate reader. The concentration for 50% growth inhibition (IC_{50}) were calculated using GraphPad Prism software.

4.5. Colony formation assays in soft agar

Compounds were diluted with 2 × McCoy's 5A or DMEM containing 20% FBS to specific concentrations. 1.2% agar and the 2 × medium were 1:1 mixed, then 1 mL of the mixture was layered onto a 35 mm petri dish. Subsequently, 0.6% agar mixed with 2 × McCoy's 5A or DMEM supplemented with 20% FBS, then 800 HCT-116 and 1200 SW480 cells were plated on top of the solidified bottom layer. For *PHGDH* knockdown or *PHGDH*-overexpressed cells, culture dishes were coated with 1 mL culture medium mixed by 1.2% agar and 2 × McCoy's 5A. Then 800 indicated cells were re-suspended in 1 mL of growth medium mixed by 0.6% agar and 2 × McCoy's 5A, then plated on top of the solidified bottom layer. The embedded cells were incubated at 37 °C and 5% CO_2 until the arising colonies were stained with 0.001% crystal violet.

4.6. Sphere formation assay and limited dilution analysis (LDA)

For sphere formation assay, 1000 HCT-116 and SW480 cells were harvested, and plated into a 96-well ultralow attachment plate (Corning) with serum-free DMEM/F12 medium containing B27 supplement, 20 ng/mL epidermal growth factor and 10 ng/ml basic fibroblast growth factor. Tumorspheres were treated with or without LXH-3-71 at indicated concentrations after 3 days of cell plating. On Day 6, the sphere numbers in each well were quantified. *PHGDH* knockdown and *PHGDH*-overexpressed cells were plated as 500 cells per well, tumorspheres numbers were counted after 3 days of incubation.

For *in vitro* LDA assay, *PHGDH* knockdown and *PHGDH*-overexpressed cells were sorted into 96-well ultralow attachment plate at densities of 62, 31, 15 or 8 cell per well. About 10 days later, wells containing spheres were counted and the results were analyzed using a web-based tool (ELDA, http://bioinf.wehi.edu.au/software/elda/index.html).

4.7. Western blotting

HCT-116 and HCT-15 cells were seeded at 3×10^5 cells/well in 6 well-plates. The cells were treated with drugs at the indicated concentrations for the appropriate times, and lysed in RIPA lysis buffer supplemented with a protease inhibitor cocktail/PMSF and dephosphorylase inhibitor NaF. The protein concentration was measured with the BCA Protein Assay Kit (Beyotime Biotechnology, P0009). Equal amounts of proteins were electrophoresed by sodium dodecyl sulfate−polyacrylamide gel electrophoresis under denaturing conditions and transferred onto the PDVF

membranes (Millipore Corp., IPVH00010). Membranes were blocked in 5% nonfat milk (BD Difco, 232100) and then incubated with primary antibodies. After being washed, the membranes were incubated with secondary antibodies and detected by a Chemiluminescence Imaging System (MiniChemi610). The following antibodies were used in this study: anti-PHGDH (14719-1-AP, Proteintech), anti-ubiquitin (10201-2-AP), anti-CD44 (15675-1-AP, Proteintech), anti-LGR5 (DF2816, Affinity), anti-CD166 antibody (21972-1-AP, Proteintech), anti-CD133 antibody (18470-1-AP), anti-CDK4 (11026-1-AP, Proteintech), anti-EGFR (sc-373746, Santa Cruz Biotechnology), anti-DDB1 (11380-1-AP, Proteintech), anti-β-actin (66009-1-Ig, Proteintech).

4.8. Biotin−streptavidin affinity pull-down assay

The pull-down assay was performed using a streptavidin-coated agarose bead (Thermo Fisher Scientific). First, the agarose beads were aliquoted and washed with PBS three times. The beads were resuspended in 1 mL of lysis buffer (20 mmol/L Tris-HCl (pH 7.4), 150 mmol/L NaCl, 10% glycerol, 1% Triton X-100), and incubated with shaking at 4 °C for 6 h with biotin probes (100 μmol/L). Next, HCT-116 cells were extracted in lysis buffer. The lysates were centrifuged at 12,000 rpm for 10 min and the suspension was kept at 4 °C. The beads were collected, washed three times with PBS, and incubated with shaking with 800 μL of the suspended cell lysate solution at 4 °C overnight. The lysate solution was removed and the beads were washed five times with wash buffer (20 mmol/L Tris-HCl (pH 7.4), 150 mmol/L NaCl, 10% glycerol, 0.1% Triton X-100), resuspended in 100 μL of 2 × sodium dodecyl sulfate (SDS) loading buffer, boiled at 100 °C for 15 min, and centrifuged at 12,000 rpm for 10 min. The supernatant was then analyzed by SDS PAGE. Specific bound proteins were excised for subsequent in-gel digestion and analysis by LC−MS/MS (Fusion).

4.9. Protein expression and purification

The full-length *PHGDH* open reading frame (Seajet Scientific, Beijing, China) was amplified by polymerase chain reaction (PCR). The PCR fragments were ligated into the pET21a (+) vector, confirmed by DNA sequencing (Genewiz, Beijing, China), and transformed to the BL21 (DE3) strain of *Escherchia coli*. Recombinant cell was cultivated at 37 °C until the OD_{600} reached 0.6−0.8. Then, PHGDH expression was induced and the cells were grown for another 18 h at 18 °C. Cells were harvested by centrifugation (5000 rpm, 10 min) and broken by sonication. Insoluble material was separated by centrifugation (16,000 rpm, 45 min) and the supernatant was purified using a nickel-nitrilotriacetic column (HisTrap HP; GE Healthcare). The protein purity was assessed by SDS-PAGE. Protein concentration was measured *via* Nanodrop 2000 (Thermo Scientific, USA)[37].

4.10. Kinase inhibition assay

The kinase activities of PHGDH were assessed using PHGDH activity assay kit (K569, BioVision).

4.11. Immunoprecipitation assay

Cells were lysed in lysis buffer (20 mmol/L Tris-HCl (pH 7.4), 150 mmol/L NaCl, 0.5% NP-40, protease inhibitor cocktail/PMSF, dephosphorylase inhibitor NaF). Lysate was incubated with 5 μg anti-PHGDH (14719-1-AP, Proteintech) or anti-DDB1 (11380-1-AP, Proteintech) antibodies and immunocomplexes were precipitated using protein A/G PLUS-Agarose (sc-2003, Santa Cruz). Immunoprecipitates were washed six times with wash buffer (20 mmol/L Tris-HCl (pH 7.4), 150 mmol/L NaCl, 0.05% NP-40, protease inhibitor cocktail/PMSF, dephosphorylase inhibitor NaF) and proteins were eluted with 2 × SDS loading buffer. The supernatant was then analyzed by SDS PAGE.

4.12. siRNA transfection

Cells were transfected with siRNAs using Lipofectamine® RNAiMAX transfection reagent (Thermo Fisher Scientific, Invitrogen, 13778075) following the manufacturer's protocol and analyzed 72 h later. siRNA knockdown efficiencies were validated by western blotting. The sequences of the siRNAs used were as follows:

siDDB1-1: 5′-UAACAUGAGAACUCUUGUC-3′;
siDDB1-2: 5′-GCAAGGACCUGCUGUUUAU-3′;
siCON: 5′-UUCUCCGAACGUGUCACGU-3′.

4.13. Microscale thermophoresis analysis

The purified PHGDH protein and PHGDH protein preincubated with LXH-3-71 (100 μmol/L) were labeled with the NT-647-NHS dye using a protein-labeling kit (NanoTemper Technologies), then diluted into 400 nmol/L with assay buffer including 0.05% Tween-20. Purified DDB1 protein (ab114333, Abcam) were diluted by two-fold and then mixed with the labeled protein 1:1 (10 μL final volume). The samples were loaded into standard capillaries (NanoTemper Technologies) and analyzed on a Monolith NT.115 MST Instrument (NanoTemper Technologies, 20% excitation power, and high MST power). The interactions were tested in three replicates.

4.14. Quantitative RT-PCR

To measure relative gene expression by qRT-PCR, total RNA was extracted using EZ-press RNA Purification Kit (EZBioscience). The cDNA was synthesized from 1 μg of total RNA by HiScript III 1st Strand cDNA Synthesis Kit (Vazyme). PCR amplification performed with the Hieff UNICON®qPCR SYBR Green Master Mix (YEASEN), and the PCR-amplified gene products were analyzed. Levels of mRNA expression were quantified after normalization to GAPDH endogenous control using the ΔCT (difference between cycle thresholds) method.

The mRNA expression of *CD133*, *CD44*, *LGR5* and *CD166* was determined by qRT-PCR. Primers used for qRT-PCR:

CD133, forward 5′-CACTACCAAGGACAAGGCGTTC-3′, reverse 5′-CAACGCCTCTTTGGTCTCCTTG-3′

CD44, forward 5′-CCAGAAGGAACAGTGGTTTGGC-3′, reverse 5′-ACTGTCCTCTGGGCTTGGTGTT-3′

CD166, forward 5′-TCCAGAACACGATGAGGCAGAC-3′, reverse 5′-GTAGACGACACCAGCAACAAGG-3′

LGR5, forward 5′-CCTGCTTGACTTTGAGGAAGACC-3′, reverse 5′-CCAGCCATCAAGCAGGTGTTCA-3′

GAPDH, forward 5′-GGAGCGAGATCCCTCCAAAAT-3′, reverse 5′-GGCTGTTGTCATACTTCTCATGG-3′

4.15. Animal study

The animal studies were approved by the Institutional Review Board of Nankai University. All animal studies were conducted

according to protocols approved by the Animal Ethics Committee of Nankai University. A total volume of 0.1 mL of PBS containing 5.0×10^6 HCT-116 cells was injected subcutaneously into six-week-old female BALB/c nude mice. When the tumor volume reached about 50−100 mm^3, the mice were randomly divided to vehicle control, 5-FU (10 mg/kg/day, i.p., $n = 5$) and LXH-3-71 (1 and 3 mg/kg/day, i.p, $n = 5$) and were treated as above dose. Mice were executed and tumors were harvested on Day 17. Ki67-positive cells and PHGDH-positive cells were staining with anti-Ki67 antibody (27309-1-AP, Proteintech) and anti- PHGDH antibody (14719-1-AP, Proteintech).

For HCT-116 intravenous xenograft, a total volume of 0.1 mL of PBS containing 1.0×10^6 HCT-116 cells with luciferase gene was injected into the tail vein of six-week-old female BALB/c nude mice. Subsequently, the mice were randomly divided into vehicle control ($n = 5$), 5-FU (10 mg/kg/day, i.p., $n = 5$), and LXH-3-71 (1 and 3 mg/kg/day, i.p., $n = 5$) and were treated as above. Bioluminescence signaling was acquired with Imaging System at Day 28 after treatment. Finally, mice were killed at Day 28, and lung tissues were harvested and fixed in 4% paraformaldehyde. Lung sections were stained with hematoxylin and eosin (H&E).

For the tumor initiation assay, a gradient of scramble or PHGDH shRNA cells (1×10^4, 1×10^5 and 1×10^6) were subcutaneously injected into Balb/c nude mice ($n = 10$). The number of tumors formed was determined 39 days post injection. On Day 39, mice were euthanized and the tumors were excised as well as weighed. CD44-positive cells and CD166-positive cells were staining with anti-CD44 antibody (15675-1-AP, Proteintech) and anti-CD166 antibody (21972-1-AP, Proteintech).

4.16. Statistical analysis

All statistical analyses were conducted using Graph Prism software. Statistically significant differences were determined by Student's *t*-test, and *P* values less than 0.05 were considered statistically significant in all cases.

Acknowledgments

This work was supported by the National Natural Science Foundation of China (NSFC, No. 82003186, 82073691 and 82373134), the International Science and Technology Cooperation Project of China (No. 2022YFE0133300), Ningbo Science and Technology Bureau under CM2025 Programme (2020Z092, China), Shenzhen Science and Technology Foundation (JCYJ20210324122006017, China), Tianjin Natural Science Fund (21JCQNJC01910, China), China Postdoctoral Science Foundation − Tianjin Joint Support Program (No. 2023T029TJ).

Author contributions

Ziqi Huang: Data curation, Formal analysis, Investigation, Methodology, Writing − original draft. Kun Zhang: Data curation, Investigation, Methodology, Writing − review & editing. Yurui Jiang: Data curation, Investigation. Mengmeng Wang: Data curation, Investigation. Mei Li: Data curation, Investigation. Yuda Guo: Data curation, Investigation. Ruolin Gao: Data curation, Formal analysis, Methodology. Ning Li: Data curation. Chenyang Wang: Data curation. Jia Chen: Data curation. Jiefu Wang: Project administration, Supervision, Writing − review & editing. Ning Liu: Data curation, Methodology, Writing − review & editing. Xiang Liu: Methodology, Supervision, Writing − review & editing. Shuangwei Liu: Methodology, Supervision, Writing − review & editing. Mingming Wei: Data curation, Project administration, Supervision, Validation, Writing − review & editing. Cheng Yang: Funding acquisition, Writing − review & editing. Guang Yang: Conceptualization, Funding acquisition, Project administration, Supervision, Writing − original draft, Writing − review & editing.

Conflicts of interest

The authors declare that they have no known competing financial interests or personal relationships that could have appeared to influence the work reported in this paper.

Appendix A. Supporting information

Supporting information to this article can be found online at https://doi.org/10.1016/j.apsb.2024.06.001.

References

1. Brenner H, Kloor M, Pox CP. Colorectal cancer. *Lancet* 2014;**383**:1490−502.
2. Li K, Wu JL, Qin B, Fan Z, Tang Q, Lu W. ILF3 is a substrate of SPOP for regulating serine biosynthesis in colorectal cancer. *Cell Res* 2019;**30**:163−78.
3. Henderson K, Kirkland SC. Multilineage differentiation of cloned HRA-19 cells in serum-free medium: a model of human colorectal epithelial differentiation. *Differentiation* 1996;**60**:259−68.
4. Vermeulen L, Todaro M, de Sousa Mello F, Sprick MR, Kemper K, Alea MP, et al. Single-cell cloning of colon cancer stem cells reveals a multi-lineage differentiation capacity. *Proc Natl Acad Sci U S A* 2008;**105**:13427−32.
5. Vermeulen L, Snippert HJ. Stem cell dynamics in homeostasis and cancer of the intestine. *Nat Rev Cancer* 2014;**14**:468−80.
6. Ricci-Vitiani L, Lombardi DG, Pilozzi E, Biffoni M, Todaro M, Peschle C, et al. Identification and expansion of human colon-cancer-initiating cells. *Nature* 2007;**445**:111−5.
7. Dalerba P, Dylla SJ, Park IK, Liu R, Wang X, Cho RW, et al. Phenotypic characterization of human colorectal cancer stem cells. *Proc Natl Acad Sci U S A* 2007;**104**:10158−63.
8. Lopez-Bertoni H, Kozielski KL, Rui Y, Lal B, Vaughan H, Wilson DR, et al. Bioreducible polymeric nanoparticles containing multiplexed cancer stem cell regulating miRNAs inhibit glioblastoma growth and prolong survival. *Nano Lett* 2018;**18**:4086−94.
9. Rasanen K, Herlyn M. Paracrine signaling between carcinoma cells and mesenchymal stem cells generates cancer stem cell niche *via* epithelialmesenchymal transition. *Cancer Discov* 2012;**2**:775−7.
10. Lenos KJ, Miedema DM, Lodestijn SC, Nijman LE, van den Bosch T, Romero Ros X, et al. Stem cell functionality is microenvironmentally defined during tumour expansion and therapy response in colon cancer. *Nat Cell Biol* 2018;**20**:1193−202.
11. Govaere O, Wouters J, Petz M, Vandewynckel YP, Van den Eynde K, Van den Broeck A, et al. Laminin-332 sustains chemoresistance and quiescence as part of the human hepatic cancer stem cell niche. *J Hepatol* 2016;**64**:609−17.
12. Wang D, Fu L, Sun H, Guo L, DuBois RN. Prostaglandin E2 promotes colorectal cancer stem cell expansion and metastasis in mice. *Gastroenterology* 2015;**149**:1884−95.e4.
13. Achouri Y, Rider MH, Schaftingen EV, Robbi M. Cloning, sequencing and expression of rat liver 3-phosphoglycerate dehydrogenase. *Biochem J* 1997;**323**:365−70.

14. Walsh DA, Sallach HJ. Purification and properties of chicken liver D-3-phosphoglycerate dehydrogenase. *Biochemistry* 1965;**4**:1076−85.
15. Snell K. Enzymes of serine metabolism in normal, developing and neoplastic rat tissues. *Adv Enzyme Regul* 1984;**22**:325−400.
16. Sharif T, Martell E, Dai C, Ghassemi-Rad MS, Lee K, Singh SK, et al. Phosphoglycerate dehydrogenase inhibition induces p-mTOR-independent autophagy and promotes multilineage differentiation in embryonal carcinoma stem-like cells. *Cell Death Dis* 2018;**9**:990.
17. Samanta D, Semenza GL. Serine synthesis helps hypoxic cancer stem cells regulate redox. *Cancer Res* 2016;**76**:6458−62.
18. Li Q, Qiu J, Yang H, Sun G, Hu Y, Zhu D, et al. Kinesin family member 15 promotes cancer stem cell phenotype and malignancy *via* reactive oxygen species imbalance in hepatocellular carcinoma. *Cancer Lett* 2020;**482**:112−25.
19. Jeon MJ, You MH, Han JM, Sim S, Yoo HJ, Lee WK, et al. High phosphoglycerate dehydrogenase expression induces stemness and aggressiveness in thyroid cancer. *Thyroid* 2020;**30**:1625−38.
20. Mullarky E, Lucki NC, Beheshti Zavareh R, Anglin JL, Gomes AP, Nicolay BN, et al. Identification of a small molecule inhibitor of 3-phosphoglycerate dehydrogenase to target serine biosynthesis in cancers. *Proc Natl Acad Sci U S A* 2016;**113**:1778−83.
21. Guo J, Gu X, Zheng M, Zhang Y, Chen L, Li H. Azacoccone E inhibits cancer cell growth by targeting 3-phosphoglycerate dehydrogenase. *Bioorg Chem* 2019;**87**:16−22.
22. Rohde JM, Brimacombe KR, Liu L, Pacold ME, Yasgar A, Cheff DM, et al. Discovery and optimization of piperazine-1-thiourea-based human phosphoglycerate dehydrogenase inhibitors. *Bioorg Med Chem* 2018;**26**:1727−39.
23. Pacold ME, Brimacombe KR, Chan SH, Rohde JM, Lewis CA, Swier LJ, et al. A PHGDH inhibitor reveals coordination of serine synthesis and one-carbon unit fate. *Nat Chem Biol* 2016;**12**:452−8.
24. Liu XH, Li BL, Zhang Z, Wei YJ, Xu ZX, Qin SL, et al. *S*ynthesis and discovery novel anti-cancer stem cells compounds derived from the natural triterpenoic acids. *J Med Chem* 2018;**61**:10814−33.
25. Todaro M, Francipane MG, Medema JP, Stassi G. Colon cancer stem cells: promise of targeted therapy. *Gastroenterology* 2010;**138**:2151−62.
26. Botchkina G. Colon cancer stem cells−from basic to clinical application. *Cancer Lett* 2013;**338**:127−40.
27. Hervieu C, Christou N, Battu S, Mathonnet M. The role of cancer stem cells in colorectal cancer: from the basics to novel clinical trials. *Cancers* 2021;**13**:1092.
28. Jackson PA, Widen JC, Harki DA, Brummond KM. Covalent modifiers: a chemical perspective on the reactivity of α,β-unsaturated carbonyls with thiols *via* hetero-Michael addition reactions. *J Med Chem* 2017;**60**:839−85.
29. Zhao Z, Liu Q, Bliven S, Xie L, Bourne PE. Determining cysteines available for covalent inhibition across the human kinome. *J Med Chem* 2017;**60**:2879−89.
30. Tan Y, Zhou X, Gong Y, Gou K, Luo Y, Jia D, et al. Biophysical and biochemical properties of PHGDH revealed by studies on PHGDH inhibitors. *Cell Mol Life Sci* 2021;**79**:27.
31. Oh S, Yeom J, Cho HJ, Kim JH, Yoon SJ, Kim H, et al. Integrated pharmaco-proteogenomics defines two subgroups in isocitrate dehydrogenase wild-type glioblastoma with prognostic and therapeutic opportunities. *Nat Commun* 2020;**11**:3288.
32. Zhao JY, Feng KR, Wang F, Zhang JW, Cheng JF, Lin GQ, et al. A retrospective overview of PHGDH and its inhibitors for regulating cancer metabolism. *Eur J Med Chem* 2018;**61**:10814−33.
33. Cho YH, Ro EJ, Yoon JS, Mizutani T, Kang DW, Park JC, et al. 5-FU promotes stemness of colorectal cancer *via* p53-mediated WNT/β-catenin pathway activation. *Nat Commun* 2020;**11**:5321.
34. Hu J, McCall CM, Ohta T, Xiong Y. Targeted ubiquitination of CDT1 by the DDB1−CUL4A−ROC1 ligase in response to DNA damage. *Nat Cell Biol* 2004;**6**:1003−9.
35. Angers S, Li T, Yi X, MacCoss MJ, Moon RT, Zheng N. Molecular architecture and assembly of the DDB1−CUL4A ubiquitin ligase machinery. *Nature* 2006;**443**:590−3.
36. Tao S, Pan S, Gu C, Wei L, Kang N, Xie Y, et al. Characterization and engineering of broadly reactive monoclonal antibody against hepatitis B virus X protein that blocks its interaction with DDB1. *Sci Rep* 2019;**9**:20323.
37. Wang Q, Liberti MV, Liu P, Deng X, Liu Y, Locasale JW, et al. Rational design of selective allosteric inhibitors of PHGDH and serine synthesis with anti-tumor activity. *Cell Chem Biol* 2017;**24**:55−65.